Responsive microcapsule reactors based on hydrogen-bonded tannic acid layer-by-layer assemblies

Veronika Kozlovskaya, Eugenia Kharlampieva, Irina Drachuk, Derek Cheng and Vladimir V. Tsukruk*

Received 4th January 2010, Accepted 6th April 2010
DOI: 10.1039/b927369g

We explore responsive properties of hollow multilayer shells of tannic acid assembled with a range of neutral polymers, poly(*N*-vinylpyrrolidone) (PVPON), poly(*N*-vinylcaprolactam) (PVCL) or poly(*N*-isopropylacrylamide) (PNIPAM). We found that properties of the nanoscale shells fabricated through hydrogen-bonded layer-by-layer (LbL) assembly can be tuned changing the interaction strength of a neutral polymer with tannic acid, and by a change in counterpart hydrophobicity. Unlike most hydrogen-bonded LbL films with two polymer components, the produced tannic acid-based multilayer shells are extremely stable in the wide pH range from 2 to 10. We demonstrate that gold nanoparticles can be grown within tannic acid-containing shell walls under mild environmental conditions paving the way for further modification of the capsule walls through thiol-based surface chemistry. Moreover, these shells show reversible pH-triggered changes in surface charge and permeability towards FITC-labeled polysaccharide molecules. The permeability of these LbL containers can be controlled by changing pH providing an opportunity for loading and release of a functional cargo under mild conditions.

Introduction

Applications in therapeutic delivery, catalysis, sensing, and biochemical reactions require a design of responsive functional materials capable of changing their properties in a controlled way under external stimuli.[1–5] Integration of responsive molecules which possess many functions offers control over response and structure of the functional hollow shells or solid core-shell structures. Among various ways, layer-by-layer assembly (LbL) is one of the prominent methods to build ultrathin polymer micro- and nanoshells with nanometre-level control over composition, thickness, and tunable chemical functionality which has been recently introduced.[6–9] In this method multiple layers are formed on various cores through a stepwise template adsorption of proper species—biological molecules, polymers, organic molecules, and nanoparticles—able to interact *via* electrostatic interactions, hydrogen-bonding or produce covalent bonds during assembly.

Hollow microcapsules can be produced by the LbL assembly onto colloid cores with charged polyelectrolytes and/or charged inorganic nanoparticles followed by subsequent decomposition of cores.[10–12] Properties of polyelectrolyte multilayer LbL microcapsules can be well controlled by changing various parameters, including pH, ionic strength, salt concentration, temperature, light, and magnetic field.[13–16] The micromechanical properties of bare or functionalized with microparticles LbL microcapsules were shown to be varied in a wide range *via* selection of polymers and fabrication conditions.[17–22] Moreover, Caruso *et al.* and Skirtach *et al.* reported the light-responsive permeability of microcapsules with gold nanoparticles encapsulated into microcapsule walls.[23,24] Spasova *et al.* reported magnetically and optically tunable LbL microcapsules.[25] Lvov and co-workers exploited magnetic field to modulate the permeability of polyelectrolyte microcapsules with gold-coated cobalt nanoparticles embedded inside the capsule walls.[26]

Several types of pH-responsive LbL systems were also introduced over a past decade. Poly(styrene sulfonate)/poly(allylamine hydrochloride) (PSS/PAH) capsules were shown to exhibit pH-controlled pore formation and healing.[27] The response mechanism of LbL assemblies was analyzed by Rubner and co-workers who attributed the dramatic variation of the swelling degree (up to 400%) to changes in the degree of ionization of weak polyelectrolytes (*i.e.*, PAH). A sharp swelling–deswelling transition detected for the LbL films at pH > 8.5 manifested itself in reversible and repeatable pH-controlled variations of swelling percentage, the surface roughness, and the refractive index. However, PSS/PAH shells exhibit pH-sensitive properties, *i.e.*, swelling, only if originally deposited under very harsh acidic or basic conditions usually incompatible with relevant ambient conditions. For instance, at extreme basic conditions, pH 9.5, PAH is partially uncharged (pK_b is 9.5–10) and therefore forms loops when interacted with PSS which can be later protonated or deprotonated in response to external pH change.[28,29] On the other hand, electrostatically LbL assembled pH-sensitive poly(methacrylic acid)/PAH (PMAA/PAH) microcapsules show a reversible size change under the extreme acidic conditions at pH 2.8.[30]

Hydrogen-bonded LbL materials present new opportunities for LbL-fabricated shells, which, otherwise, could be more difficult to realize. Most of hydrogen-bonded systems studied to date have been demonstrated to be unstable and dissolve under physiological conditions thus facilitating degradability but compromising mid-term stability.[31,32] Their properties offer fabrication of nano- and micro-containers responsive in

School of Materials Science and Engineering, Georgia Institute of Technology, Atlanta, Georgia, 30332, USA. E-mail: Vladimir@mse.gatech.edu

biologically and physiologically relevant pH range under mild environmental conditions. Thus, the hydrogen-bonded LbL assembly of films and shells in water allows incorporating uncharged biocompatible functional polymers within the LbL film such as poly(ethylene oxide) (PEO), known to be resistant to protein and lipid adsorption, which is crucial for use in biomedical applications. Another example of non-toxic and biocompatible material is poly(*N*-vinylpyrrolidone) (PVPON), which has been demonstrated to be a key component for numerous designs and can facilitate conversion of hydrogen-bonded LbL films into single- or two-component ultrathin hydrogel materials with responsive, low-fouling or/and biodegradable properties.[33–37]

Along with pH-/salt-responsive properties, hydrogen-bonded hollow capsules of poly(*N*-vinylcaprolactam) (PVCL) and poly(*N*-isopropylacrylamide) (PNIPAM) have shown much promise for temperature-responsive drug delivery under physiological conditions.[38] For example, an uncharged PVCL component with lower critical solution temperature (LCST) of 36 °C can be assembled with PMAA and resultant LbL multilayers exhibit distinct temperature-responsive changes in dye permeability. Dye-release properties of hydrogen-bonded multilayer assemblies of temperature responsive PNIPAM and poly(acrylic acid) (PNIPAM/PAA) at various temperatures have been explored earlier by Caruso and co-workers.[39,40]

The dissolution pH is highly dependent on the particular polymer counterpart selection used for LbL assembly, reflecting the strength of binding of a particular polymer pair.[41] The pH-triggered mechanism of hydrogen-bonded capsule dissolution yet can be utilized for a fast release of container contents. However, some potential biomedical or bio-sensing applications of hydrogen-bonded LbL materials require their stability over a broad pH range and transformation under mild conditions which have been rarely demonstrated.

Interest to tannic acid (TA) as a molecule with the ability to multiple hydrogen bonding due to the presence of numerous terminal hydroxyl groups has been spiked relatively recently due to its high biological activity including antioxidant, antimicrobial, anticarcinogenic, antimutagenic and antibacterial properties.[42–44] The anticarcinogenic and antimutagenic potentials of polyphenols are related to their antioxidative property in protecting cellular components from oxidative damage. It is due to unique functional structure of tannic acid, which possesses maximum number of hydroxyl groups compared to other derivatives of tannins, the antioxidant properties of TA are revealed.[45] As reported, polyphenols possess high ability to reduce free-radicals and inhibit radical-induced oxidation of adjacent molecules.[46–48]

It is important to note that tannic acid is not a true acid molecule because it does not contain the carboxyl groups (–COOH) which are present in all organic acids. Instead, it is defined as a polyphenol, a compound with many phenol (C_6H_5OH) groups. TA molecule consists of three digallic acid units directing to one side of the glucose core and two other digallic acid units to the opposite side (Fig. 1).[49] The phenolic content of TA is expressed by the number of galloyl groups attached to the glucose molecule. A large number of carbonyl and phenolic functional groups are responsible for different types of bonding with various molecules which includes a combination

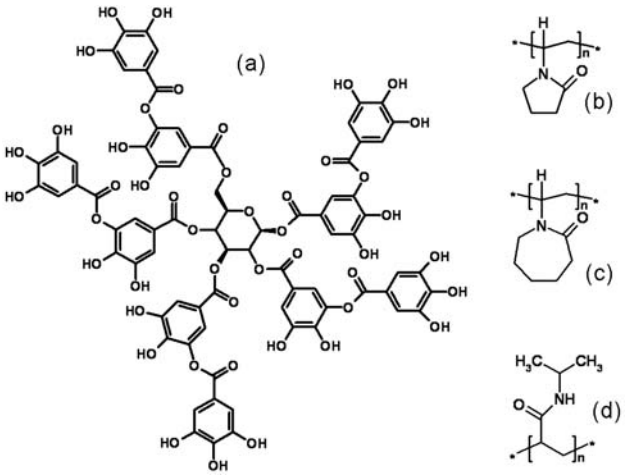

Fig. 1 Chemical structures of tannic acid (a) used in the hydrogen-bonded LbL assembly with poly(*N*-vinylpyrrolidone) (b), poly(*N*-vinylcaprolactam) (c), and poly(*N*-isopropylacrylamide) (d).

of hydrogen bonding, hydrophobic interactions, electrostatic interaction, and covalent bonding associated with oxidation.[50] Binding tannic acid with various bio-molecules has been shown to be pH- and temperature dependent.[51,52] The affinities are weaken only at high temperatures but remain unaffected by pH variations between 3.8 and 6.0.

Previous work has been focused on LbL-constructed multilayers on the basis of tannic acid combined with typical synthetic polyelectrolytes such as PAH, poly(diallyldimethylammonium chloride) (PDDA), 90% quaternized poly(*N*-vinylpyridine) (Q90) and naturally derived polyelectrolyte chitosan.[53,54] Polyphenols ionically assembled with polyelectrolytes retained their ability to scavenge free radicals.[48] The results of the previous works suggested that polyphenol multilayers organized as protective coatings on the surface of biodevices or compacted drugs can inhibit or diminish free-radical damage of encapsulated compound. Shutava *et al.* has reported that multilayer capsules of polyphenols assembled with amine-based polyelectrolytes (PAH and PDDA) demonstrated selective pH permeability.[53] Minimal permeability of polysaccharides was observed between pH 5 and 7, with a maximum in permeability achieved at either low or high pH.[53] Different threshold permeability was observed in LbL microcapsules composed of TA and chitosan, which was shifted to lower pH 3 and pH 5 as compared to conventional PAH/PSS capsules.[55] Similarly, the authors also demonstrated the effect of molecular weight of encapsulated substances on permeability of $(TA/chitosan)_4$ microcapsules with bovine serum albumin loaded in and released from the capsules by a pH-triggered manipulation of the TA/chitosan capsules.

Despite the promising new properties of LbL assemblies of tannic acid, a little is known about the hydrogen-bonded assembly of tannic acid with non-ionic polymers. Several neutral polymers, such as PVPON, PEO, PVCL, PNIPAM have been investigated as potential pH-stable materials for sustain release formulations.[56,57] It has been demonstrated that critical dissolution pH for decomposition of the polymeric films can be drastically higher when tannic acid assembled with the neutral polymers instead of highly charged polymers. The nature of

neutral polymer is important for tuning the dissolution pH of tannic acid multilayers from neutral to basic conditions.

In contrast to previous published studies, we explored tannic acid based hydrogen-bonded systems from another perspective focusing on properties of the free-standing TA-based microcapsules. We investigated how changes in the nature and molecular weight of the neutral polymer, the strength of its interaction with tannic acid and a change in counterpart hydrophobicity affect the surface properties of the produced TA/PVPON, TA/PVCL, TA/PNIPAM LbL shells and, consequently, the responsive properties of the (TA/neutral polymer) microcapsules. The novel twist of our work is pH-triggered permeability of the stable free-standing TA-based systems which can be simply tuned by the change in the intermolecular interactions. Finally, another novel finding of this work is the capability of TA-based shells for *in situ* gold nanoparticle synthesis within the shells due to the presence of tannic acid. In contrast to our previous work on hydrogel capsules, the TA-based capsules do not require additional cross-linking to achieve necessary stability and functionalities (*e.g.* amino groups) for gold reduction. Thus, we explore the redox-active properties of TA molecules in bound state to chelate and reduce metal ions facilitating *in situ* synthesis of gold nanoparticles inside the shells.

In seeking answers to these questions, atomic force microscopy (AFM), scanning electron microscopy (SEM), confocal laser scanning microscopy (CLSM), zeta-potential measurements, and *in situ* attenuated total reflection Fourier-transform infrared spectroscopy (ATR-FTIR) were utilized to elucidate the topography characteristics and responsive properties of the novel TA-based hydrogen-bonded LbL shells. We believe that the obtained information is essential for understanding the mechanism of hydrogen-bonded interactions in the thin films. Despite the fundamental interest, the optimization of capsule composition by varying polymer molecular weight and chemistry is a crucial parameter for the capsule performance as responsive microcontainers with desired physical properties. Besides, the capability of the capsules to reduce gold opens a new avenue to fabricate environmentally-neutral responsive hybrid materials at ambient environmental conditions.

Results and discussion

Surface properties of (TA/polymer) capsules

At initial stage, we varied molecular weight and nature of a neutral polymer to check if this can affect surface properties of the shells. Fig. 1 shows chemical structures of TA and neutral polymers, *i.e.*, PVPON, PVCL and PNIPAM which are exploited in this study.

Fig. 2 depicts overall principles of the microcapsule design exploited in this work. The shell fabrication was applied to silica spherical templates. Two routes of the multilayer formation were explored in our study. The silica surfaces can be pre-coated with poly(ethyleneimine) (PEI) layer to ensure good adhesion of the following (TA/polymer) LbL multilayer to the particle surfaces. In the other route, we employed the direct formation of the (polymer/TA) LbL multilayers on silica surfaces through hydrogen-bonding interactions of PVPON, PVCL or PNIPAM components with the hydroxyl-terminated silica surface.[58]

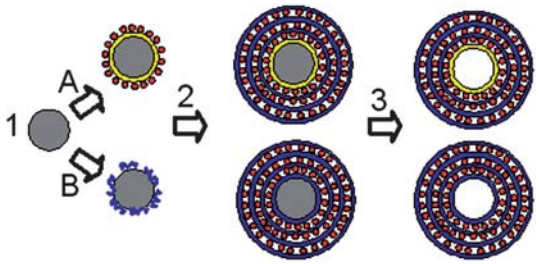

Fig. 2 General schematics of the LbL (TA/non-ionic polymer) capsules formation based on hydrogen-bonding. Silica microparticles (1) are used as sacrificial templates. Hydrogen-bonded (TA/non-ionic polymer) coatings can be formed either through deposition on PEI-treated silica particles (1A) starting from TA or through direct deposition of the (non-ionic polymer/TA) multilayer starting from a neutral polymer (1B). When a desired number of the bilayers is achieved (2), silica cores are etched out leaving behind hollow capsules (3).

We were able to successfully fabricate TA-based LbL hollow capsules at pH = 5 (0.01 M) with all non-ionic polymers used in this work. Fig. 3a demonstrates that robust and well-separated TA/PVPON hollow capsules with no sign of capsule aggregation can be produced after completely etching out silica cores. After being placed on a silicon wafer, the capsules have been collapsed upon drying with many random folds caused by local instabilities and wrinkling due to capillary forces acting on the microcapsules (Fig. 3b).[59]

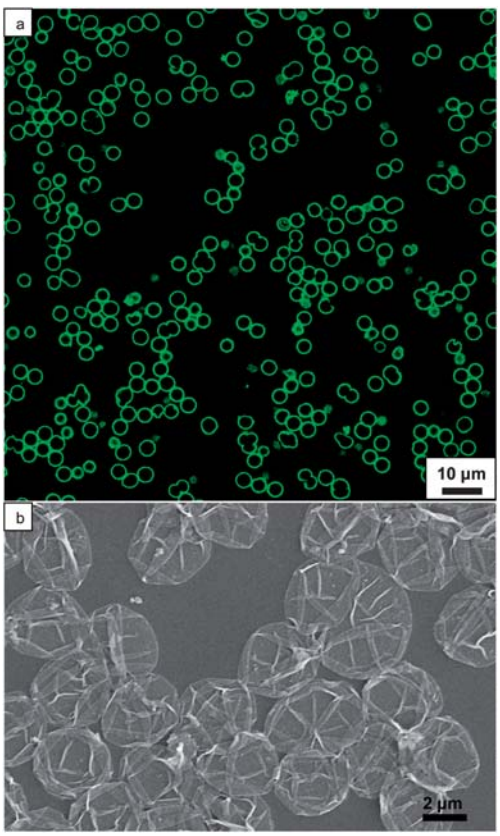

Fig. 3 The CLSM image of PEI-$(TA/PVPON)_3$ capsules in aqueous solution (a) and the SEM image of dried hollow PEI-$(TA/PVCL)_4$ capsules collapsed on silicon wafer.

The surface morphology of the obtained capsules was then analyzed with AFM (Fig. 4). The AFM analysis of the dried hollow TA/PVPON capsules shown in Fig. 4 revealed a grainy surface morphology of the folded shells in all three studied TA/PVPON systems. The microroughness of 5.6 ± 0.3 nm, 5.2 ± 0.3 nm and 5.4 ± 0.2 nm was measured for different capsules when the molecular weight of PVPON was 55 000 Da, 360 000 Da and 1 300 000 Da, respectively (here and below measured at 1 × 1 μm^2 areas). These values are higher than common values for ionic-based LbL films (usually below 1 nm) and reflect local aggregation of the polymer components.[60,61] In fact, hydrogen-bonded multilayers are usually reported to have higher

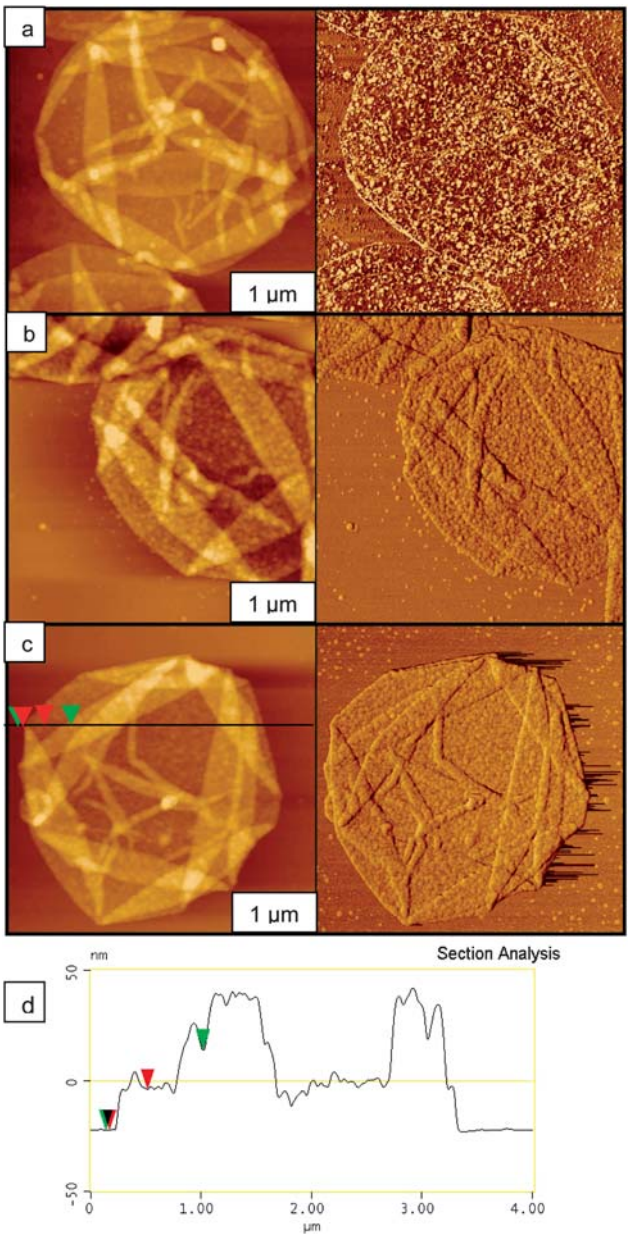

Fig. 4 AFM topography (left) and phase images (right) of PEI-(TA/PVPON)$_4$ capsules prepared from PVPON with M_w = 55 000 (a), M_w = 360 000 (b), and M_w = 1 300 000 (c). *Z*-scale is 100 nm for topography images. Section analysis of the PEI-(TA/PVPON-1300)$_4$ capsule is shown in (d).

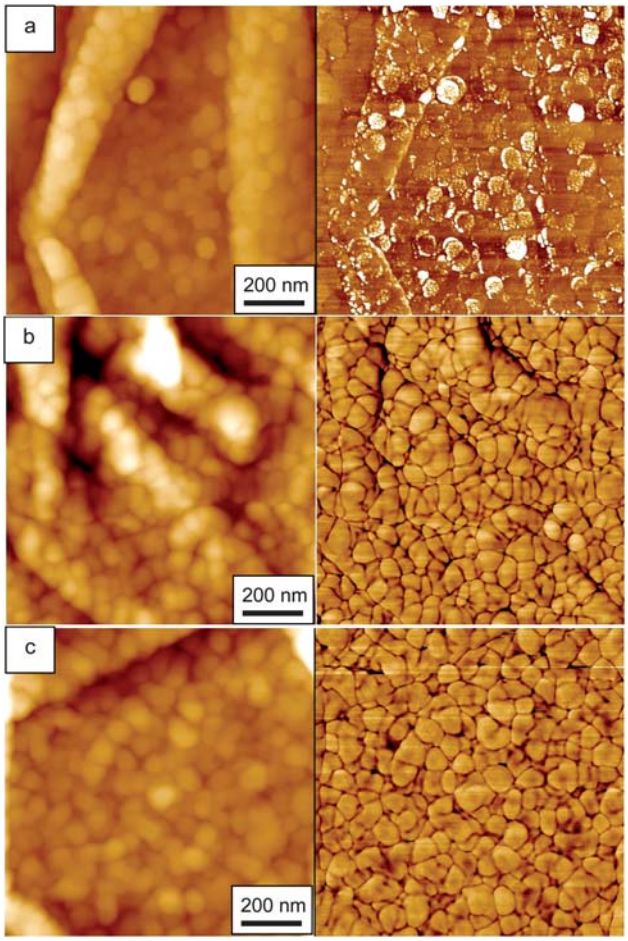

Fig. 5 AFM topography (left) and phase (right) images of the PEI-(TA/PVPON)$_4$ capsules prepared from PVPON with M_w = 55 000 (a), M_w = 360 000 (b), and M_w = 1 300 000 (c). *Z*-scale is 80 nm for all topography images.

microroughness of several nanometres with the values dependent on fabrication conditions.[62] AFM images obtained with the higher magnification demonstrate the presence of larger TA/PVPON domains of aggregated polymer layers (close to 100 nm) regardless of the molecular weight of PVPON component (Fig. 5).

We explored the effect of molecular weight of a neutral polymer, *i.e.*, PVPON or PVCL, on the properties of the (TA/non-ionic polymer) multilayers assembled at pH = 5. Interestingly, the change in the molecular weight from 55 000 Da to 1 300 000 Da resulted in a doubled bilayer thickness of a single TA/PVPON wall and increased from 1.0 ± 0.1 nm to 2.2 ± 0.2 nm, respectively (Table 1). AFM analysis of the domains revealed a slight increase in the domain height in the case of higher molecular weight of PVPON from 5 ± 2 nm for the (TA/PVPON-55)$_4$ to 8 ± 2 nm for the (TA/PVPON-360)$_4$ and to 8 ± 2 nm for the (TA/PVPON-1300). These results reflect the increase in the overall thickness for TA/PVPON systems, probably due to an increased amount of binding sites for longer PVPON chains.

Similar trend was observed for the TA/PVCL LbL system: the average bilayer thickness increased from 3.5 ± 0.2 nm to 4.2 ± 0.1 nm with the increased molecular weight of PVCL from

Table 1 Average thicknesses of a bilayer for (TA/non-ionic polymer) LbL multilayers built on surfaces of either silica microparticles or on silicon wafers

	Average bilayer thickness, nm	
LbL multilayers[a]	Capsules	Films
TA/PVPON-55	1.0 ± 0.1	1.2 ± 0.1
TA/PVPON-360	1.5 ± 0.2	2.3 ± 0.2
TA/PVPON-1300	2.2 ± 0.2	3.5 ± 0.4
TA/PVCL-2	3.5 ± 0.2	n/a
TA/PVCL-70	4.2 ± 0.1	
TA/PNIPAM-20	5.7 ± 0.3	n/a

[a] In all systems, a pre-layer of PEI was first adsorbed on the surface.

2000 Da to 70 000 Da. It is worth noting that (TA/polymer) systems assembled on silica particles resulted in systematically thinner films compared to those deposited on planar silicon wafers. For instance, TA/PVPON planar LbL films assembled from PVPON with $M_w = 55\,000$ Da and with $M_w = 1\,300\,000$ Da led to an increased bilayer thickness. The respective bilayer thickness values are 1.0 ± 0.1 nm and 2.2 ± 0.2 nm for the shells fabricated on silica cores which are lower than that for the planar films (Table 1). The observed lowering in the average bilayer thickness for hydrogen-bonded films adsorbed on particulate substrates compared to that on planar ones was reported earlier and was attributed to the difference in the deposition conditions for two methods.[63,64] Moreover, direct deposition of (TA/polymer) films onto the silicon substrate without using a PEI precursor layer, always resulted in slightly thicker (from 20% to 40%) films because of the absence of the ionization of TA molecules. As known, in contrast, TA molecules are partially charged due to the presence of charged PEI.[65]

We observed similar but less pronounced effect of the molecular weight of PVCL on surface morphology of the TA/PVCL capsules (Fig. 6). The PEI-(TA/PVCL)$_4$ capsules composed either from PVCL with $M_w = 2000$ Da or with $M_w = 70\,000$ Da exhibited slightly smoother surface morphology with the microroughness of 3.9 ± 0.3 nm and 4.1 ± 0.2 nm, respectively (Fig. 6a and 6c). The PEI pre-layer used to enhance the hydrogen-bonded multilayer adhesion to the substrate surface had a negligible effect on the surface properties of the TA/PVCL shells. Both PEI-(TA/PVCL-70) and (TA/PVCL-70) multilayers exhibited similarly smooth surface morphology regardless of the present PEI pre-layer, showing the microroughness of 4.1 ± 0.2 nm and 4.2 ± 0.2 nm, respectively. The virtually identical microroughness of 3.9 ± 0.3 nm and 4.0 ± 0.2 nm was obtained for PEI-(TA/PVCL-2) and (TA/PVCL-2) multilayers.

The drastic difference was found in the surface topography of the capsules, when the hydrophobicity of the non-ionic counterpart was changed (Fig. 7). A less grainy surface morphology was achieved when PNIPAM or PVCL was used instead of PVPON with the microroughness slightly decreasing from 5.6 ± 0.3 nm for the (TA/PVPON-55)$_4$ to 5.0 ± 0.2 nm for (TA/PNIPAM-20)$_4$ and to 4.1 ± 0.2 nm for (TA/PVCL-70)$_4$ capsules. These results can be explained by increased strength of interaction between TA and a polymer within the (TA/polymer) LbL multilayers which led to observed smoothening of the TA-containing LbL films. The increase in hydrophobicity of the neutral polymer for previously reported poly(carboxylic acid)/neutral polymer hydrogen-bonded systems resulted in higher pH-stability when poly(methacrylic acid)/PVCL (PMAA/PVCL) was used instead of PMAA/PNIPAM pair.[41]

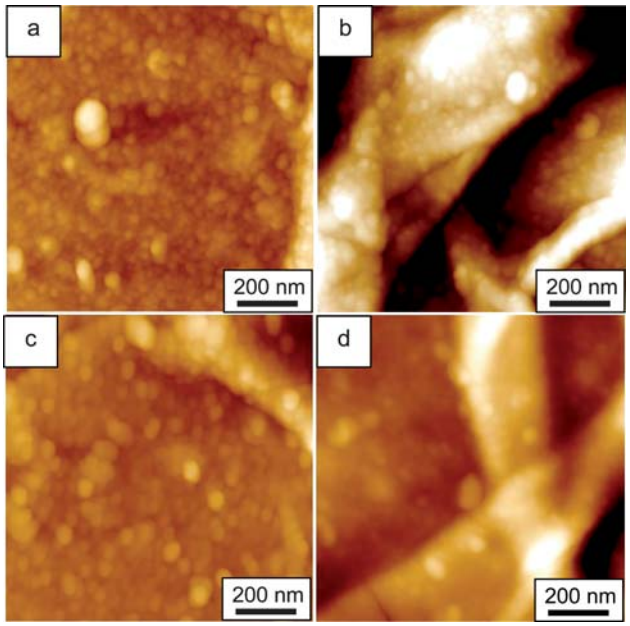

Fig. 6 AFM topography images of PEI-(TA/PVCL-70)$_4$ (a), (PVCL-70/TA)$_4$ (b), PEI-(TA/PVCL-2)$_4$ (c), and (PVCL-2/TA)$_4$ (d). *Z*-scale is 100 nm for all images.

pH-Triggered control over properties of TA/PVPON shells

We pursued the fabrication of TA-based hydrogen-bonded capsules at a slightly acidic pH = 5 to design shells with pH responsive properties stable under biologically relevant conditions. It is worth mentioning that in the case of planar films it is important to ensure the pH-stability of the pre-layers used to enhance the initial adsorption. In some cases, weakened interactions of the enhancing pre-layer and the substrate can result in the detachment of the multilayer from the substrate leading to wrong conclusions about the multilayer pH-stability.

The pH-stability of planar films of the TA/PVPON or TA/PVCL composed from polymers of similar molecular weights at lower pH, *i.e.*, pH = 2, had been reported to have the critical dissolution pH of ~9 and ~9.5, respectively.[56] To verify if there is any effect of the polycation pre-layer on the pH-stability of the (TA/polymer) LbL hydrogen-bonded systems, we carried out capsule fabrication with or without a PEI precursor layer.

Firstly, the deposition of TA/PVPON multilayers was performed at pH = 5 onto silica particles pre-coated with PEI (Fig. 2, route A). Typically, 1.2 ± 0.8 nm of PEI was adsorbed under these conditions. The strong interaction of the first TA layer with PEI is facilitated *via* ionic pairing of positively charged PEI (pK_a = 9.5 for primary amines, pK_a = 7 for secondary amines)[66] with slightly negatively charged phenolic groups of TA. Although the estimated pK_a values for phenolic groups is reported to be in the pH region from 5 to 8.5, the increased ionization of TA phenol groups was also reported in the vicinity of positively charged polyelectrolyte chains.[67,68]

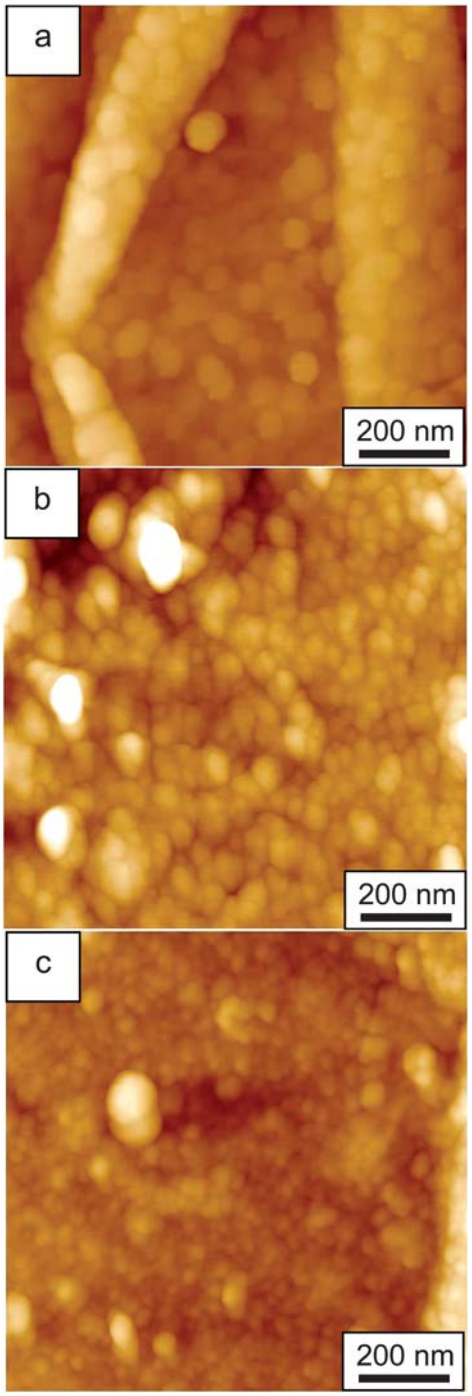

Fig. 7 AFM topography images of PEI-(TA/PVPON-55)$_4$ (a), PEI-(TA/PNIPAM-20)$_4$ (b), and PEI-(TA/PVCL-70)$_4$ (c). *Z*-scale is 100 nm for all images.

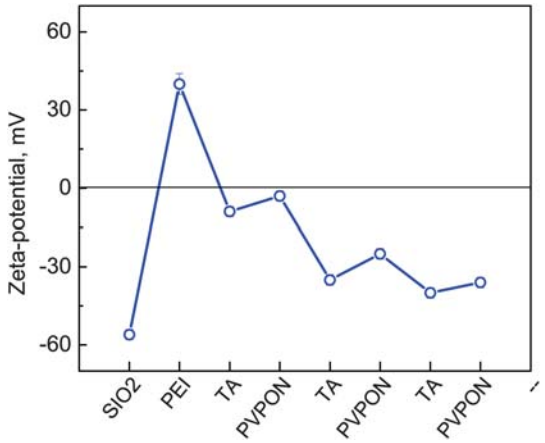

Fig. 8 Evolution of zeta-potential during deposition of PEI-(TA/PVPON)$_3$ multilayer on surfaces of silica particles in aqueous solution at pH = 5.

Fig. 8 demonstrates the evolution of the surface charges of capsules during LbL formation of PEI-(TA/PVPON-55)$_3$ on silica particles. After PEI deposition, the zeta-potential of the capsules switches from -56 ± 2 mV for silica surface due to ionized silanol groups (pK_0 and pK_a of surface silanol groups are 2–3 and 9.1–9.4, respectively[69]) to $+40 \pm 4$ mV due to adsorbed positively charged polycation chains. Such surface charge reversal is typically observed in electrostatic LbL assembly of oppositely charged polymers at surfaces.[70] However, in contrast to the regular LbL assembly of conventional polyelectrolytes, the LbL formation of the following hydrogen-bonded TA/PVPON is characterized by the overall negative zeta-potential throughout the entire multilayer formation due to the ionized phenolic groups of TA molecules.

During the deposition steps of PVPON component, the decrease in the negative value of the zeta-potential was observed to be -6 mV. Similar oscillations of the zeta-potential within negative values were reported for hydrogen-bonded multilayers of poly(carboxylic acid)s[65,64] and were explained by the shifting of the effective slip plane, at which electrophoretic mobility and the zeta-potential is measured, away from the surface. Such a shift occurs due to immobilization of water associated with the polymer loops when uncharged polymer adsorbs onto a charged surface.[71] On the other hand, the absence of the charge reversal along with the presence of negative surface charge throughout the entire deposition allows a good stability of the particle suspension and prevents it from severe aggregation. The charge-mediated stability of the polymer-coated particles is crucial for the fabrication of well-separated capsules (Fig. 3a).

In the second route, direct deposition of the PVPON/TA LbL multilayers onto silica surfaces without a PEI-treatment was performed at pH = 2 (Fig. 2, route B). In this case, PVPON was adsorbed first because of hydrogen bonds formed between protonated silanols of the silica surface and carbonyl groups on PVPON chains.[72,73] When hollow PEI-(TA/PVPON)$_3$ or (PVPON/TA)$_3$ capsules were transferred from pH = 5 to pH = 10, no capsule dissolution was observed (Fig. 9). There was also no distinctive change in the capsule diameter. For instance, PEI-(TA/PVPON)$_3$ capsules exhibited the diameter of 2.8 ± 0.2 μm at pH =5 and 2.9 ± 0.2 μm at pH = 10 (Fig. 8a, 8b). The hydrogen-bonded capsule shells did not show pH-dependent swelling typical for the polyelectrolyte capsules under conditions when charge balance within a shell is disturbed. In such a case, the excess of either charge is introduced within the shell under extreme pH close to pK_a values of the polyelectrolytes.[29] The observed phenomenon can be explained by the fact that TA is a small and relatively rigid molecule with permanent molecular

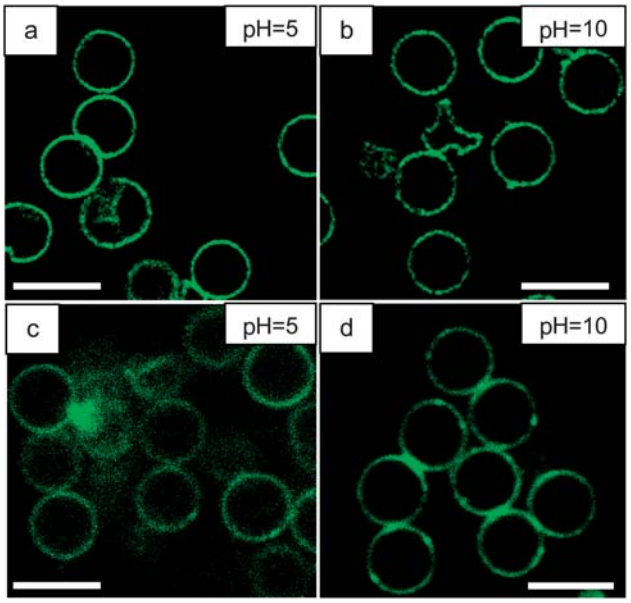

Fig. 9 Confocal images of (TA-PVPON-55)$_4$ capsules at pH 5 (a) and pH 10 (b) and PEI-(TA-PVPON-55)$_4$ at pH 5 (c) and pH 10 (d). Scale bar is 5 μm for all images.

dimensions unable to swell upon the pH changes unlike flexible and long-chain synthetic poly(carboxylic acid)s.[74,75]

Such high pH-stability seems surprising especially if we consider the pK_a of TA is in the range from pH = 5 to pH = 8.5.[67] Quick disassembly of the hydrogen-bonded PMAA/PVPON or PAA/PVPON usually occurs when such multilayers are brought to pH close to a pK_a value of the ionizable counterpart.[31] On the other hand, increased association strength of hydrogen-bonded components due to cooperative hydrophobic interactions was observed for higher molecular weights of a polymer component. This effect resulted in overall increase of the film pH-stability and a shift of a critical dissolution pH to higher pH values.[41]

The emerging negative charges in response to pH increase were observed for PEI-(TA/PVPON)$_3$ capsules composed from PVPON with M_w = 55 000 Da. Fig. 10 shows that indeed the magnitude of the negative surface charge of the PEI-(TA/PVPON) capsules increased after their exposure to the basic pH and became −55 ± 2 mV at pH = 9 *versus* −36 ± 2 mV at pH = 6 reflecting the appearance of ionized phenolic groups within the capsule shells. However, it is evident that the magnitude of such increase is lower when PVPON with higher molecular weight was used for the capsule shell fabrication. This difference is probably reflective of better negative charge screening by longer PVPON chains and consistent with the thicker TA/PVPON-1300 shells with the same number of deposited layers (Table 1). The better charge screening, in turn, can be due to a suppressed ionization because of a larger number of binding sites in the case of longer PVPON chains.[41]

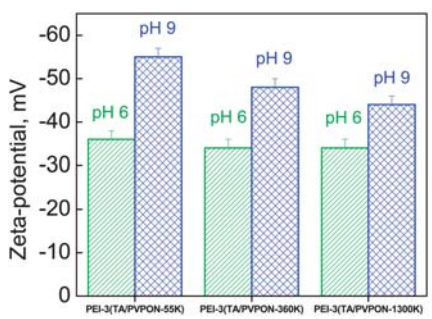

Fig. 10 Variations of ζ-potential values of the hollow PEI-(TA/PVPON)$_3$ capsules made of PVPON with M_w = 55 000 Da, 360 000 Da, and 1 300 000 Da and exposed to aqueous solutions at pH 6 or pH 9.

To understand if any compositional changes occur within the shell upon the pH change from pH = 5 to pH = 9, *in situ* ATR-FTIR experiments were additionally performed. For these measurements, the PEI-(TA/PVPON)$_5$ LbL films were built on a silicon crystal in a flow-through cell, and their pH-triggered changes were monitored in real-time (Fig. 11). The important feature of the ATR-FTIR technique is its ability to monitor individual components of the layered films with very few layers and track compositional changes by following the characteristic functional groups.

Fig. 11a demonstrates that the FTIR spectrum of the LbL film at pH = 5 is similar to that at pH = 9 with four major absorbance bands which are easily resolved. The O–H stretching frequencies for the phenolic groups are located in the 3180–3400 cm^{-1} region.[76] An adsorption band at 1718 cm^{-1} is associated with C═O stretching vibration of the ester groups in TA molecule

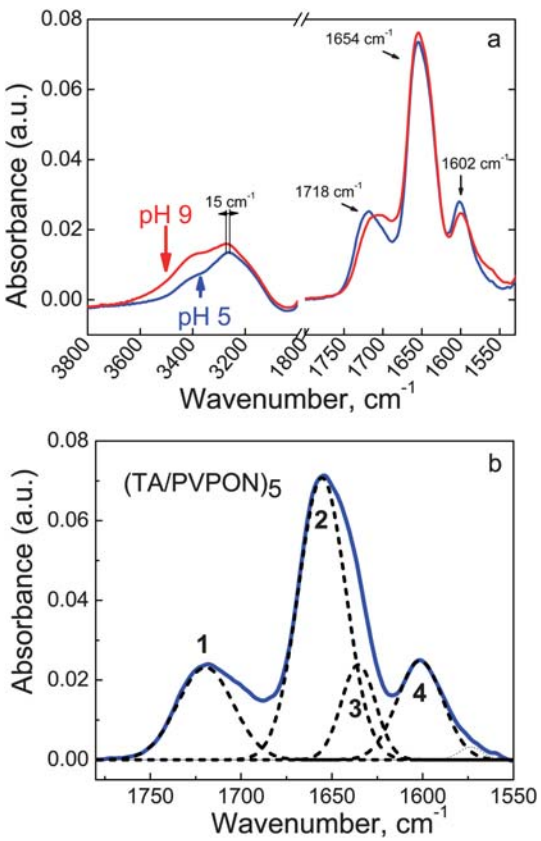

Fig. 11 ATR-FTIR spectra of PEI-(TA/PVPON-55)$_5$ films deposited on silicon crystal from 0.01M phosphate buffer solutions at pH 5 and exposed to pH 9 (a) with the peak deconvolution for the film deposited at pH = 5 (b).

and a strong adsorption band at 1654 cm^{-1} originates from stretching vibrations of carbonyl groups of the pyrrolidone ring[77] overlapped with the stretching vibrations from TA aromatic rings (Fig. 11b, see peaks 2 and 3).[56] Another absorption peak of aromatic ring stretch vibrations appears at ~1602 cm^{-1}.[56]

In our experiments, the peak at 1718 cm^{-1} shifted to 1704 cm^{-1} along with the O–H stretch band shift from 3258 cm^{-1} to 3273 cm^{-1} when the $(TA/PVPON)_5$ LbL film was exposed to pH = 9. These changes reflect the disruption of hydrogen-bonds of carbonyl and hydroxyl groups in LbL multilayers. As known, such a disruption causes a displacement of the frequencies of the stretch absorption of the carbonyl towards lower wavenumbers up to 20 cm^{-1} while in the case of hydroxyl groups such shift occurs upwards up to 300 cm^{-1}.[78,79] Importantly, the presence of the adsorption band at 1654 cm^{-1} at both pH = 5 and pH = 9 indicates that there is no PVPON released from the film upon the pH change. The observed high capability of TA/PVPON films to withstand an internal ionization within the multilayer can be explained by the ability of TA to form intra-molecular hydrogen bonds. Such stabilizing effect can be enhanced with the increase of a number of participating phenolic units.[53]

pH-Controlled permeability of TA/PVPON hydrogen-bonded capsules

We employed confocal microscopy to reveal if the observed changes in capsule shell might affect the permeability properties of the TA/PVPON capsules (Fig. 12). The capsule permeability was monitored by using FITC-dextrans of various molecular weights as a fluorescent probe. Capsules were considered impermeable for the probe if the ratio of intensities from capsule interior to bulk solution was less than 0.5 during 15 min after the fluorescent probe solution was mixed with capsules as has been suggested in the literature.[80–82,53] Table 2 compares the permeability of the dextrans through the TA/PVPON shells made of various molecular weight PVPON polymers.

Fig. 12 shows that the $(TA/PVPON\text{-}55)_4$ shells exposed to pH = 6 demonstrate a highly permeable, "open" structure for the dextrans of up to 250 000 Da, being "closed" only for the dextran with M_w = 500 000 Da (Fig. 12a, 12b). High molecular weight permeants (M_w > 500 000 Da) are rejected by the $(TA\text{-}PVPON\text{-}55)_4$ capsules at pH = 6, which is close to the fabrication conditions of the shells when they bear some negative charge (Fig. 12c). The dextran permeability through the shells decreased with stronger bound multilayers of the $(TA/PVPON\text{-}360)_4$ and $(TA/PVPON\text{-}1300)_4$. In those cases, the shells were capable of excluding dextrans of M_w < 40 000 Da (Table 2). These results correlate well with the data on the thicker shells of $(TA/PVPON\text{-}360)_4$ and $(TA/PVPON\text{-}1300)_4$ compared to that of TA/PVPON-55 (Table 1).

The permeability of dextrans through the shells decreased when pH was switched from slightly acidic pH 6 to basic pH 9 (Table 2). This permeability profile is in contrast to previously

Table 2 Permeability of $PEI\text{-}(TA/PVPON\text{-}55)_4$, $PEI\text{-}(TA/PVPON\text{-}360)_4$, $PEI\text{-}(TA/PVPON\text{-}1300)_4$ capsules to FITC-labeled dextrans with different molecular weights and at pH 6 and 9

	Capsules					
Permeant	$PEI\text{-}(TA/PVPON\text{-}1300)_4$		$PEI\text{-}(TA/PVPON\text{-}360)_4$		$PEI\text{-}(TA/PVPON\text{-}55)_4$	
Dextran, M_w	pH 6	pH 9	pH 6	pH 9	pH 6	pH 9
4 kD	+[a]	—	+	+	+	+
10 kD	+	—	+	+	+	+
20 kD	+	—	+	–	+	+
40 kD	—	—	–	–	+	+
70 kD	—	–	–	–	+	–
150 kD	—	–	–	–	+	–
250 kD	—	–	–	–	+	–
500 kD	–	–	–	–	–	–

[a] Symbols "+" and "–" indicate capsule permeability and impermeability, respectively after 15 min of observation.

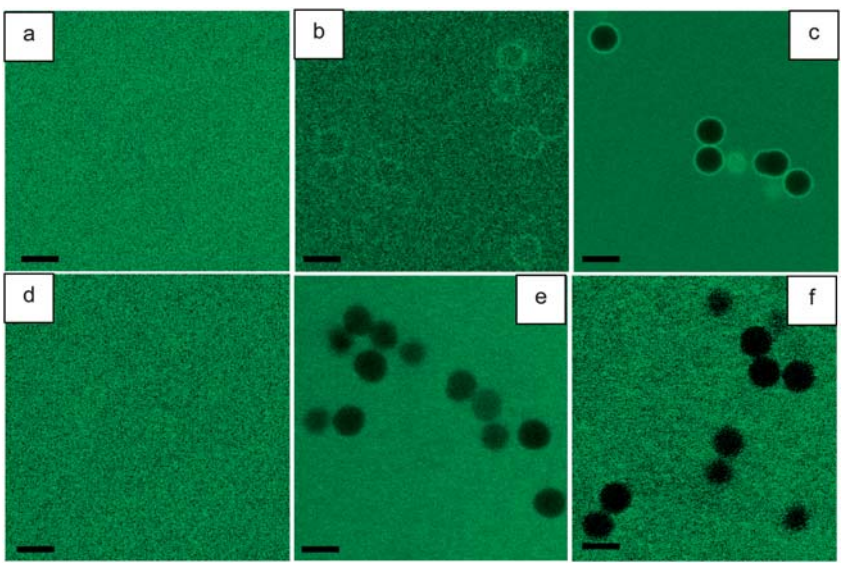

Fig. 12 Confocal microscopy images of $PEI\text{-}(TA/PVPON\text{-}55)_4$ capsules in phosphate buffer solution at pH 6 (top images) and at pH 9 (bottom images) exposed to FITC-dextran solution with M_w = 4000 (a, d), M_w = 70 000 (b, e), M_w = 500 000 (c, f). Scale bar is 4 μm.

studied permeability of TA/PAH or TA/PDDA ionically paired multilayer LbL capsules which showed the lowest permeability in the pH region from 5 to 7.[53] Fig. 12 illustrates that the $(TA/PVPON\text{-}55)_4$ capsules became impermeable for the dextran of 70 000 Da when pH was changed from 6 to 9 (Fig. 12b and 12e, respectively).

Under basic pH conditions similar trend of the decreased dextran permeability was observed when PVPON with $M_w = 55\,000$ Da was changed to that with $M_w = 360\,000$ Da or $M_w = 1\,300\,000$ Da (Table 2). In the case of ionically paired TA/PAH or TA/PDDA capsules, the pH-dependent permeability was attributed to slow dissolution of the capsules under basic pH.[53] However, in the case of the hydrogen-bonded TA/PVPON capsules stable within $2 < pH < 10$ range, the observed decrease in the shell permeability most probably reflects structural changes within the capsule shells. We suggest that the phenomenon is related to the disruption of intra-molecular hydrogen bonds of TA molecules at basic pH as discussed above. However, further studies would be necessary to elucidate the mechanism of the changes in permeability observed in this study.

Growth of gold nanoparticles within TA/PVPON capsule walls

We next took advantage of the phenolic groups available in tannic acid molecules which is known to act both as a strong chelating agent for metal ions[83–85] and a reductant of noble metal ions.[86,87] Recently we have demonstrated that gold nanoparticles can be directly grown within hydrogel-layered PMAA capsules.[88] The nanoparticle synthesis was possible only when free amine groups were introduced within shells during chemical cross-linking of the capsules which were capable of binding tetrachloroaurate ions.

TEM analysis of the $PEI\text{-}(TA/PVPON\text{-}55)_3$ capsules after their exposure to $HAuCl_4$ solution in the borate buffer revealed the presence of monodisperse gold nanoparticles with narrow size distribution (standard deviation below 20%) and the average size of 4 nm (Fig. 13a, 13b). Fig. 13c shows the solution absorption spectrum of the $(TA/PVPON\text{-}55)_3$-Au capsules which additionally confirms the presence of the reduced gold nanoparticles. The energy dispersive spectroscopy (EDS) confirms the presence of gold nanoparticles in the hollow shells (Fig. 13d). Gold nanostructures are known to exhibit distinctive SPR features which depend on their shape and size.[89] The spectrum has an absorbance peak around 530 nm corresponding to the SPR of gold nanoparticles with the diameter below 50 nm which is in good agreement with the TEM analysis.[90]

When PVPON with larger molecular weight was used to assemble TA/PVPON capsules, gold nanoparticles with broader size distribution were produced inside $PEI\text{-}(TA/PVPON\text{-}360)_3$ LbL shells (Fig. 14). Under these conditions, gold nanoparticles have been grown with the average particle size of 8 ± 5 nm, which is almost two times larger than that for $PEI\text{-}(TA/PVPON\text{-}55)_3$–Au (Fig. 13b). Moreover, in the case of $PEI\text{-}(TA/PVPON\text{-}1300)_3$ capsules, we observed a broad distribution of the diameters with two most probable diameters at 3 ± 1 nm and 10 ± 2 nm (Fig. 14b).

Based on these results, it is clear that the particle size is dependent on the amount of (tannic acid/PVPON) present within the shells which is consistent with the thicker (TA/PVPON) shells made of higher molecular weight of PVPON discussed above. On the other hand, PVPON is known to play a crucial role in the

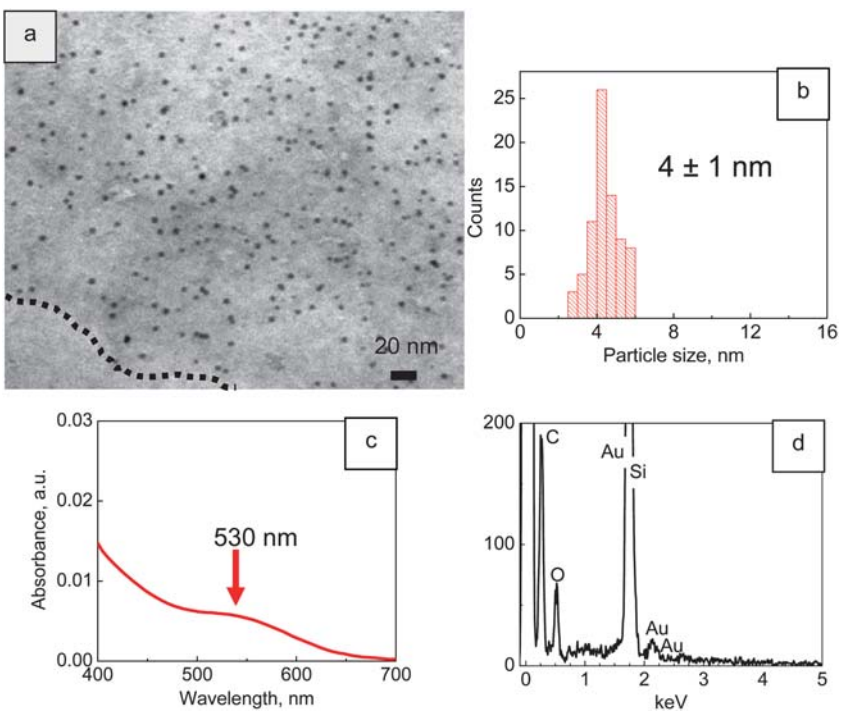

Fig. 13 The TEM image of $PEI\text{-}(TA/PVPON\text{-}55)_3$-Au hollow capsule (a) with the particle size distribution (b) and the UV-vis spectrum of $PEI\text{-}(TA/PVPON\text{-}55)_3$-Au capsule solution (c). The EDX data for the $PEI\text{-}(TA/PVPON\text{-}55)_3$-Au capsules (d). The dashed line in (a) shows the edge of the capsule.

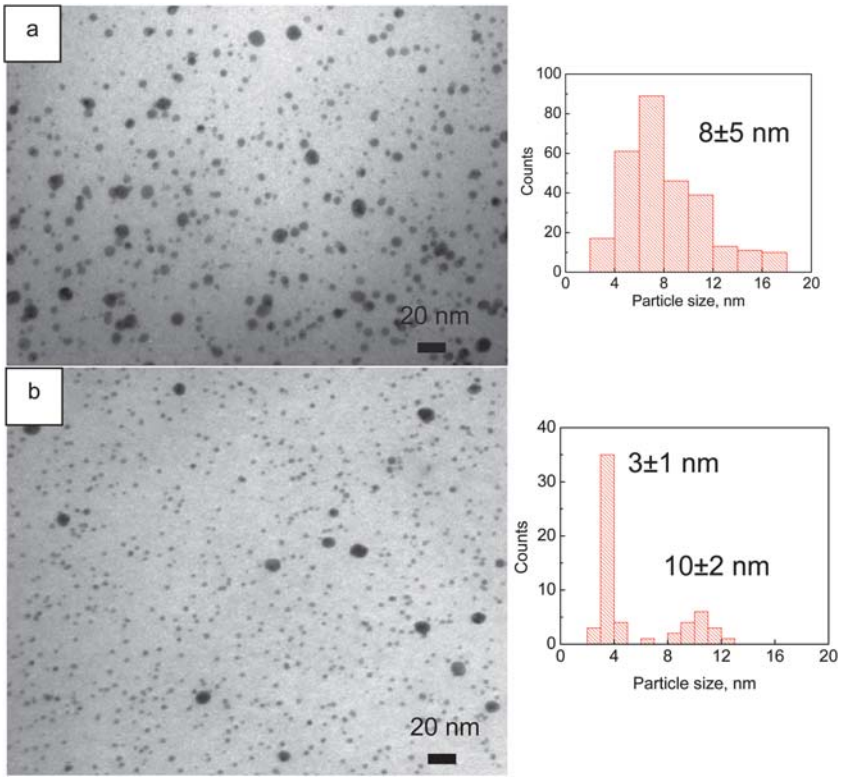

Fig. 14 TEM images of PEI-(TA/PVPON-360)$_3$-Au (a) and PEI-(TA/PVPON-1300)$_3$–Au hollow capsules (b) with the gold particle size distributions.

nanoparticle growth by blocking the facet of metal as a capping polymer agent.[91,92] Seemingly, the thicker TA/PVPON shells can lead to more available reducing sites on tannic acid resulting in larger nanoparticles produced in (TA/PVPON-360) shells (Fig. 14a). The increasing amount of PVPON, however, can be responsible for appearance of a second peak of much smaller particles (3 ± 1 nm) when Au^{3+} is reduced within the TA/PVPON-1300 system, while the non-ionic polymer serves as a good stabilizer for the particles not allowing particle aggregation.

Conclusions

We utilized the hydrogen-bonded LbL assembly to successfully fabricate hollow shells of TA/PVPON, TA/PVCL and TA/PNIPAM multilayers. The shell thickness of the produced capsules ranged from 6 nm to 12 nm for PEI-(TA/PVPON-55)$_5$ and PEI-(TA/PVPON-1300)$_5$ capsules, respectively, with the respective average bilayer thickness ranging from 1 nm to 2.2 nm. The thickness of the shell can be controlled by changing the molecular weight of the non-ionic counterpart or by increasing the strength of association between TA and a polymer. This opportunity is important for the hydrogen-bonded systems as this allows varying the bilayer thickness in the system of the same chemical composition without changing a number of deposited polymer pairs. In contrast, for ionically assembled LbL shells, it is necessary to change the deposition conditions, *e.g.*, pH or ionic strength, to achieve the similar effect. However, in this case such changes may undermine the stability of the coated particles and consequently result in their poor stability in solution.

We found no pronounced effect of a charged pre-layer on the formation of the shells and, more importantly, on the responsive properties of the (TA/polymer) shells which is beneficial for the use of these systems on substrates regardless of their surface charge due to the fact that PEI can be used as a universal precursor. We provide additional confirmation of the unusually high pH-stability of the hydrogen-bonded (TA/polymer) shells in the pH range from 2 to 10 regardless of the presence/absence of pre-layer. Increase in the internal ionization and in negative shell surface charge evidenced by the ATR-FTIR spectroscopy and zeta-potential measurements do not result in shell disassembly in contrast to vast majority of hydrogen-bonded LbL shells based on poly(carboxylic acids).

We found that permeability of dextran molecules through the LbL shells can be regulated by varying the molecular weight of the non-ionic counterpart. The lowest permeability for the same dextran was achieved by increasing PVPON molecular weight and can be attributed to increased association between the counterparts and can be tuned by pH-triggered disruption of intra-molecular hydrogen bonds of TA molecules. Finally, the chelating and reducing properties of TA were used to produce gold nanoparticles within the hydrogen-bonded TA/PVPON shells. We suggest that these properties of the (TA/polymer) shells show the straightforward way for the fabrication of environmentally-neutral and responsive hybrid shells at ambient conditions.

We believe that *in situ* growth of gold nanoparticles within the hydrogen-bonded TA-based polymer shells is an elegant way to obtain corresponding inorganic–organic biologically active nanostructures as gold possesses good biocompatibility and

optical plasmon resonances which can be easily colorimetrically monitored. Moreover, various antibodies and proteins can be readily conjugated through thiol-based surface chemistry or electrostatic binding. These properties of the reported shells can find a potential use for the fabrication of responsive ultrathin yet robust microcapsules for biochemical sensing and detection as well as laser- or chemically-induced cargo release for biotechnology applications.

Experimental

Materials

Tannic acid (TA) (M_w = 1700 Da), polyethyleneimine (PEI) (M_w = 25 000 Da), poly(*N*-vinylpyrrolidone, M_w = 55 000 Da (PVPON-55), M_w = 360 000 Da, (PVPON-360), M_w = 1 300 000 Da, (PVPON-1300), poly(*N*-isopropylacrylamide) (PNIPAM) (M_w = 20 000 Da), mono- and dibasic sodium phosphate were purchased from Sigma-Aldrich. Poly(*N*-vinylcaprolactam), M_w = 70 000 Da (PVCL-70), M_w = 2000 Da (PVCL-2), and silica particles with diameter of 4.0 ± 0.2 μm as 10% dispersions in water were obtained from Polysciences, Inc. Hydrofluoric acid (48–51%) was purchased from BDH Aristar. Ultrapure (Nanopure system) filtered water with a resistivity of 18.2 MΩ cm was used in all experiments. Single-side polished silicon wafers of the {100} orientation (Semiconductor Processing Co.) were cut by typical size of 10 × 20 mm and cleaned in a piranha solution as described elsewhere.[93]

Fabrication of PEI-(TA/neutral polymer)$_n$ capsules and films

The LbL deposition of hydrogen-bonded multilayers of (TA/neutral polymer) on particulate substrates has been performed according to the established procedure.[6] Briefly, 0.5 mg mL^{-1} polymer solutions were prepared by dissolving polymers in 0.01 M sodium phosphate buffer with pH adjusted to 5, except for PEI, which was dissolved in 0.1 M NaCl with pH adjusted to 7. Typical deposition time was 15 min followed by three rinsing steps in phosphate buffer solution (0.01 M, pH = 5) to remove excess of polymer. The hydrogen-bonded multilayers of (TA/neutral polymer) were deposited onto silica microparticles or silicon wafers by two routs. In the first route, a pre-layer of branched-PEI was adsorbed first followed by alternate adsorption of (TA/PVPON) multilayer starting with TA. In the second route, direct deposition of (PVPON/TA) multilayer was performed on particulate or planar substrates at pH = 2 starting from a neutral polymer. For particle suspensions, after each deposition step they were settled down by centrifugation at 2000 rpm for 2 min to remove the excess of polymer. Deposition, rinsing and re-suspending steps were performed on a VWR analog vortex mixer at 2000 rpm. To etch out silica cores, the microparticles with the deposited multilayers were exposed to 8% hydrofluoric acid solution (HF) overnight followed by dialysis in ultra-pure water for 36 h with repeated change of water. Deposition of hydrogen-bonded multilayers on silicon wafers was performed by dipping a substrate into an appropriate solution followed by three rinsing steps in 0.01M phosphate buffer (pH = 5).

Growth of gold nanoparticles within TA/PVPON multilayer capsules

For growth of gold nanoparticles within the shells, 0.5 mL suspensions of silica cores with the deposited multilayers were exposed to the borate buffers to activate tannic acid for 15 min. After that the particle solution was centrifuged and supernatant was removed followed by addition of 2 mL of 1.6 mM $HAuCl_4$ solution in 0.1 M borate buffer. The solution was then left for 12 h in the dark. After gold reduction, the particle suspensions were centrifuged and extensively rinsed with water. Silica cores were dissolved in HF solution as described above to produce hollow gold-containing capsules.

UV-visible spectroscopy (UV-Vis)

UV-visible spectra of the LbL films and hollow shell solutions were recorded using a UV-2450 spectrophotometer (Shimadzu). Experiments were carried out in 1.5 mL semi-microplastic cuvettes (PlastiBrand, Germany) with 10 mm optical path.

Ellipsometry measurements

Film assembly as well as the film thickness before and after exposure to different pH values were determined using a M-2000U spectroscopic ellipsometer (Woollam). Prior to the measurements, samples were dried with a stream of nitrogen.

Atomic force microscopy (AFM)

Surface morphology of the hollow capsules and films was examined using atomic force microscopy (AFM). AFM images were collected using a Dimension-3000 (Digital Instruments) microscope in the "light" tapping mode according to the well established procedure.[94] For capsule sample preparation, a drop of capsule suspension was placed onto a pre-cleaned silicon wafer and dried in air prior to AFM imaging. For film thickness measurements the capsule single wall thickness was determined as half of the height of the collapsed flat regions of dried capsules bearing analysis from NanoScope software to generate height histograms.[95]

Transmission electron microscopy (TEM)

TEM was performed on a JEOL 1200EX electron microscope operated at 100 kV. To analyze the nanoparticle-containing capsules, they were placed on a carbon-coated gold grid (Electron Microscopy Sciences) and dried in air before TEM analysis.

Scanning electron microscopy (SEM)

SEM imaging of hollow capsules was performed on Hitachi S-3400-II scanning electron microscope with electric current of 10 kV in vacuum (<1 Pa). Before imaging, capsules were let air-dried on silicon wafers and then sputter-coated with gold.

ζ-Potential measurements

Deposition of TA/PVPON layers on silica particles was followed and the ζ-potentials measurements of PEI-(TA/PVPON) capsules at pH = 6 and pH = 9 were performed on Zetasizer

Nano-ZS equipment (Malvern). The pH values of aqueous capsule solutions were adjusted using 0.01 M HCl or NaOH solutions. Each value was obtained by averaging three independent measurements of 40 sub-runs each.

Confocal laser scanning microscopy (CLSM)

Confocal images of capsules were obtained with an LSM 510 UV Vis laser scanning microscope (Zeiss, Germany) equipped with C-Apochromat 63× oil immersion objective. If necessary, capsules were visualized through addition of the Alexa Fluor 488 dye to a capsule solution. The excitation/emission wavelengths were 488/515 nm. To check a pH-stability of the capsules, a drop of a dispersion of hollow capsules was added to several Lab-Tek chambers (Electron Microscopy Sciences), which were then filled with buffer solutions at a certain pH. Capsules were allowed to settle down and then analyzed. To investigate the pH effect on capsule permeability to FITC-dextrans, a drop of a dispersion of hollow capsules was added to several Lab-Tek chambers, which were then half-filled with buffer solutions at a certain pH and ionic strength and then mixed with FITC-dextrans (1 mg mL^{-1}) at the same pH values adjusted with 0.1 M NaOH. CLSM images of the capsules were taken after 15 min and averaged for 20 individual capsules.

Attenuated total reflection-fourier transform infrared spectroscopy (ATR-FTIR)

In situ ATR-FTIR during deposition and exposure of the TA/PVPON LbL coatings to various pH conditions was done with a Bruker FTIR spectrometer Vertex 70 equipped with a narrow-band mercury cadmium telluride detector.[96,97] The ATR surface was rectangular trapezoidal multiple reflection Si or Ge crystals of dimension 50 mm × 10 mm × 2 mm (Harrick Scientific) whose beam entrance and exit surfaces were cut at 45 degrees. Interferograms were collected at 4 cm^{-1} resolution, and the number of averaged scans was 120. Each interferogram was corrected on the corresponding background, measured for the same ATR cell with the same D_2O buffer solution. The bare ATR crystal was used as a background. To eliminate overlap of the IR bands in the 1700–1500 cm^{-1} region with the strong water band, D_2O with 99.9% isotope content was utilized. Multilayer films of PEI-$(TA/PVPON)_5$ were deposited on a hydrophilic silicon crystal *in situ* within the flow-through ATR-FTIR liquid cell: 0.5 mg mL^{-1} solutions of a polycation in 0.01 M buffer in D_2O were adsorbed onto the surface of the oxidized silicon crystal at appropriate pH for 15 min, and after that the polymer solution was replaced by pure buffer solution in D_2O without polymer. TA was then deposited from 0.5 mg mL^{-1} solution at pH = 5 followed by PVPON solution of the same concentration and the deposition cycle was repeated. The absorption peaks were analyzed with Galactic Grams/32 software as described elsewhere.[98]

Acknowledgements

This work is supported by the Air Office of Scientific Research FA9550-08-1-0446 project, FA9550-09-1-0162, and NSF-CBET-NIRT 0650705 grants. We are grateful to Prof. Nils Kröger (Georgia Institute of Technology) for providing the facility for zeta-potential measurements.

References

1 I. Tokarev and S. Minko, *Soft Matter*, 2009, **5**, 511–524.
2 P. M. Mendes, *Chem. Soc. Rev.*, 2008, **37**, 2512–2529.
3 I. Luzinov, S. Minko and V. V. Tsukruk, *Prog. Polym. Sci.*, 2004, **29**, 635–698.
4 M. C. Stuart, W. Huck, J. Genzer, M. Müller, C. Ober, M. Stamm, G. Sukhorukov, I. Szleifer, V. V. Tsukruk, M. Urban, F. Winnik, S. Zauscher, I. Luzinov and S. Minko, *Nat. Mater.*, 2010, **9**, 101–113.
5 C. Jiang and V. V. Tsukruk, *Adv. Mater.*, 2006, **18**, 829–840.
6 K. Breitenkamp and T. Emrick, *J. Am. Chem. Soc.*, 2003, **125**, 12070–12071.
7 R. Tangirala, Y. Hu, M. Joralemon, Q. Zhang, J. He, T. P. Russell and T. Emrick, *Soft Matter*, 2009, **5**, 1048–1054.
8 F. Caruso, R. A. Caruso and H. Mohwald, *Science*, 1998, **282**, 1111–1114.
9 E. Donath, G. B. Sukhorukov, F. Caruso, S. E. Davis and H. Mohwald, *Angew. Chem., Int. Ed.*, 1998, **37**, 2201–2205.
10 A. A. Antipov and G. B. Sukhorukov, *Adv. Colloid Interface Sci.*, 2004, **111**, 49–61.
11 G. B. Sukhorukov, A. L. Rogach, B. Zebli, T. Liedl, A. G. Skirtach, K. Köhler, A. A. Antipov, N. Gaponik, A. S. Susha, M. Winterhalter and W. J. Parak, *Small*, 2005, **1**, 194–200.
12 S. Srivastava and N. Kotov, *Acc. Chem. Res.*, 2008, **41**, 1831–1841.
13 B.-S. Kim and O. I. Vinogradova, *J. Phys. Chem. B*, 2004, **108**, 8161–1865.
14 W. Tong, W. Dong, C. Gao and H. Möhwald, *J. Phys. Chem. B*, 2005, **109**, 13159–13165.
15 W.-F. Dong, S. Liu, L. Wan, G. Mao, D. G. Kurth and H. Möhwald, *Chem. Mater.*, 2005, **17**, 4992–4999.
16 B.-S. Kim, O. V. Lebedeva, K. Koynov, H. Gong, G. Glasser, I. Lieberwith and O. I. Vinogradova, *Macromolecules*, 2005, **38**, 5214–5222.
17 B.-S. Kim, T.-H. Fan, O. V. Lebedeva and O. I. Vinogradova, *Macromolecules*, 2005, **38**, 8066–8070.
18 K. Kohler, H. Mohwald and G. B. Sukhorukov, *J. Phys. Chem. B*, 2006, **110**, 24002–24010.
19 K. Kohler, D. G. Shchukin, H. Mohwald and G. B. Sukhorukov, *J. Phys. Chem. B*, 2005, **109**, 18250–18259.
20 R. Mueller, K. Kohler, R. Weinkamer, G. Sukhorukov and A. Fery, *Macromolecules*, 2005, **38**, 9766–9771.
21 A. Fery and R. Weinkamer, *Polymer*, 2007, **48**, 7221–7235.
22 M. F. Bedard, A. Munoz-Javier, R. Mueller, P. del Pino, A. Fery, W. J. Parak, A. G. Skirtach and G. B. Sukhorukov, *Soft Matter*, 2009, **5**, 148–155.
23 A. S. Angelatos, B. Radt and F. Caruso, *J. Phys. Chem. B*, 2005, **109**, 3071–3076.
24 A. G. Skirtach, C. Dejungnat, D. Braun, A. S. Susha, A. L. Rogach, W. J. Parak, H. Möhwald and G. B. Sukhorukov, *Nano Lett.*, 2005, **5**, 1371–1377.
25 M. Spasova, V. Salgueiriño-Maceira, A. Schlachter, M. Hilgendorff, M. Giersig, L. M. Liz-Marzán and M. Farle, *J. Mater. Chem.*, 2005, **15**, 2095–2098.
26 Z. Lu, D. P. Malcolm, Z. Guo, V. O. Golub, C. S. S. R. Kumar and Y. M. Lvov, *Langmuir*, 2005, **21**, 2042–2050.
27 A. A. Antipov, D. Shchukin, Y. Fedutik, I. Zanaveskina, V. Klechkovskaya, G. Sukhorukov and H. Mohwald, *Macromol. Rapid Commun.*, 2003, **24**, 274–277.
28 J. Hiller and M. F. Rubner, *Macromolecules*, 2003, **36**, 4078–4083.
29 C. Dejugnat and G. B. Sukhorukov, *Langmuir*, 2004, **20**, 7265–7269.
30 T. Mauser, C. Dejugnat and G. Sukhorukov, *Macromol. Rapid Commun.*, 2004, **25**, 1781–1785.
31 E. Kharlampieva, V. Kozlovskaya and S. A. Sukhishvili, *Adv. Mater.*, 2009, **21**, 3053.
32 J. F. Quinn, A. P. R. Johnston, G. K. Such, A. N. Zelikin and F. Caruso, *Chem. Soc. Rev.*, 2007, **36**, 707–718.
33 A. S. Hoffman, *Adv. Drug Delivery Rev.*, 2002, **54**, 3–12.
34 A. N. Zelikin, Q. Li and F. Caruso, *Chem. Mater.*, 2008, **20**, 2655–2661.
35 A. N. Zelikin, A. L. Becker, A. P. R. Johnston, K. L. Wark, F. Turatti and F. Caruso, *ACS Nano*, 2007, **1**, 63–69.

36 V. Kozlovskaya, E. Kharlampieva, I. Erel and S. A. Sukhishvili, *Soft Matter*, 2009, **5**, 4077–4087.
37 C. R. Kinnane, G. K. Such, G. Antequera-Garcıa, Y. Yan, S. J. Dodds, L. M. Liz-Marzan and F. Caruso, *Biomacromolecules*, 2009, **10**, 2839–2846.
38 E. Kharlampieva, V. Kozlovskaya, J. Tyutina and S. A. Sukhishvili, *Macromolecules*, 2005, **38**, 10523–10531.
39 J. Quinn and F. Caruso, *Langmuir*, 2004, **20**, 20–22.
40 J. Quinn and F. Caruso, *Macromolecules*, 2005, **38**, 3414–3419.
41 E. Kharlampieva and S. A. Sukhishvili, *J. Macromol. Sci.: Polymer Reviews*, 2006, **46**, 377–395.
42 T. G. Shutava, S. S. Balkundi, O. Vangala, J. J. Steffan, R. L. Bigelow, J. A. Cardelli, D. P. O'Neal and Y. M. Lvov, *ACS Nano*, 2009, **3**, 1877–1885.
43 K. M. Riedl and A. E. Hagerman, *J. Agric. Food Chem.*, 2001, **49**, 4917.
44 G. K. B. Lopes, H. M. Schulman and M. Hermes-Lima, *Biochemica et Biophysica Acta*, 1999, **1472**, 142–152.
45 N. S. Khan, A. Ahmad and S. M. Hadi, *Chem.-Biol. Interact.*, 2000, **125**, 177–189.
46 D. M. Hushulian, V. A. Fechina, S. V. Kazakov, I. Y. Sakharov and I. G. Gazaryan, *Biochemistry*, 2003, **68**, 1006–1011.
47 J. Takebayashi, A. Tai and I. Yamamoto, *Biol. Pharm. Bull.*, 2003, **26**, 1368–1370.
48 T. G. Shutava, V. E. Agabekov and Y. M. Lvov, *Russ. J. Gen. Chem.*, 2007, **77**, 1494–1501.
49 D. Lin and B. Xing, *Environ. Sci. Technol.*, 2008, **42**, 5917–5923.
50 K.-T. Chung, T. Y. Wong, C.-I. Wei, Y.-W. Huang and Y. Lin, *Crit. Rev. Food Sci. Nutr.*, 1998, **38**, 421–464.
51 A. E. Hagerman, M. E. Rice and N. T. Ritchard, *J. Agric. Food Chem.*, 1998, **46**, 2590–2595.
52 A. J. Charlton, N. J. Baxter, M. L. Khan, A. J. G. Moir, E. Haslam, A. P. Davies and M. P. Williamson, *J. Agric. And Food Chemistry*, 2002, **50**, 593–1601.
53 T. G. Shutava, M. Prouty, D. Kommireddy and Y. Lvov, *Macromolecules*, 2005, **38**, 2850–2858.
54 T. G. Shutava, M. D. Prouty, V. E. Agabekov and Y. M. Lvov, *Chem. Lett.*, 2006, **35**, 1144–1145.
55 T. G. Shutava and Y. M. Lvov, *J. Nanosci. Nanotechnol.*, 2006, **6**, 1655–1661.
56 I. Erel-Unal and S. A. Sukhishvili, *Macromolecules*, 2008, **41**, 3962–3970.
57 I. Erel-Unal and S. A. Sukhishvili, *Macromolecules*, 2008, **41**, 8737–8744.
58 V. Kozlovskaya and S. A. Sukhishvili, *Macromolecules*, 2006, **39**, 6191–6199.
59 C. Jiang, S. Singamaneni, E. Merrick and V. V. Tsukruk, *Nano Lett.*, 2006, **6**, 2254–2259.
60 S. Markutsya, C. Jiang, Y. Pikus and V. V. Tsukruk, *Adv. Funct. Mater.*, 2005, **15**, 771–780.
61 C. Jiang, S. Markutsya and V. V. Tsukruk, *Langmuir*, 2004, **20**, 882–890.
62 V. Kozlovskaya, E. Kharlampieva, B. P. Khanal, P. Manna, E. R. Zubarev and V. V. Tsukruk, *Chem. Mater.*, 2008, **20**, 7474–7485.
63 V. Kozlovskaya, S. Ok, A. Sousa, M. Libera and S. A. Sukhishvili, *Macromolecules*, 2003, **36**, 8590–8592.
64 S. Y. Yang, D. Lee, R. E. Cohen and M. F. Rubner, *Langmuir*, 2004, **20**, 5978–5981.
65 V. Kozlovskaya, S. Yakovlev, M. Libera and S. A. Sukhishvili, *Macromolecules*, 2005, **38**, 4828–4836.
66 E. Tsuchida and J. Nishikawa, *J. Polym. Sci., Polym. Chem. Ed.*, 1976, **14**, 1557–1560.
67 D. Lin, N. Liu, K. Yang, Z. Zhu, Y. Xu and B. Xing, *Carbon*, 2009, **47**, 2875–2882.
68 E. Kharlampieva and S. A. Sukhishvili, *Langmuir*, 2003, **19**, 1235–1243.
69 S. A. Sukhishvili and S. Granick, *J. Chem. Phys.*, 1998, **109**, 6861–6868.
70 G. B. Sukhorukov, E. Donath, H. Lichtenfeld, E. Knippel, M. Knippel, A. Budde and H. Mohwald, *Colloids Surf., A*, 1998, **137**, 253–266.
71 L. K. Koopal and J. Lyklema, *Faraday Discuss. Chem. Soc.*, 1975, **59**, 230–241.
72 V. Kozlovskaya and S. A. Sukhishvili, *Macromolecules*, 2006, **39**, 6191–6199.
73 V. Kozlovskaya, A. Shamaev and S. A. Sukhishvili, *Soft Matter*, 2008, **4**, 1499–1507.
74 K. Ariga, A. Vinu, M. Miyahara, J. P. Hill and T. Mori, *J. Am. Chem. Soc.*, 2007, **129**, 11022–11023.
75 D. Pristinski, V. Kozlovskaya and S. A. Sukhishvili, *J. Chem. Phys.*, 2005, **122**, 014907.
76 D. Lin-Vien, N. B. Colthup, W. G. Fateley, G. G. Grasselli, *The Handbook of Infrared and Raman Characteristics Frequencies of Organic Molecules*, Academic Press, Boston, 1991, pp. 45–57.
77 V. Kozlovskaya, E. Kharlampieva, M. Mansfield and S. A. Sukhishvili, *Chem. Mater.*, 2006, **18**, 328–336.
78 F. Cangelosi and M. T. Shaw, *Polym. Eng. Sci.*, 1983, **23**, 669–675.
79 S. A. Sukhishvili and S. Granick, *Macromolecules*, 2002, **35**, 301–310.
80 W. Tong, C. Gao and H. Mohwald, *Chem. Mater.*, 2005, **17**, 4610–4616.
81 W. Tong, C. Gao and H. Mohwald, *Macromolecules*, 2006, **39**, 335–340.
82 A. A. Antipov, G. B. Sukhorukov, S. Leporatti, I. L. Radchenko, E. Donath and Mohwald, *Colloids Surf., A*, 2002, **198–200**, 535–541.
83 E. Matuschek and U. Svanberg, *J. Food Sci.*, 2002, **67**, 420–424.
84 M. Brune, L. Hallberg and A. B. Skanberg, *J. Food Sci.*, 1991, **56**, 128–131.
85 M. Brune, L. Rossander and L. Hallberg, *Eur. J. Clin. Nutr.*, 1989, **43**, 547–557.
86 H. M. Chen, C. F. Hsin, J. F. Lee and L. Y. Jang, *J. Phys. Chem.*, 2007, **111**, 5909–5914.
87 S. L. Cumberland and G. F. Strouse, *Langmuir*, 2002, **18**, 269–276.
88 V. Kozlovskaya, E. Kharlampieva, S. Chang, R. Muhlbauer and V. V. Tsukruk, *Chem. Mater.*, 2009, **21**, 2158–2167.
89 B. Wang, K. Chen, S. Jiang, F. Reincke, W. Tong, D. Wang and C. Y. Gao, *Biomacromolecules*, 2006, **7**, 1203–1209.
90 S. Link and M. A. El-Sayed, *J. Phys. Chem. B*, 1999, **103**, 4212–4217.
91 Y. Sun and Y. Xia, *Science*, 2002, **298**, 2176–2180.
92 T. S. Ahmadi, Z. L. Wang, T. C. Green, A. Henglein and M. A. El-Sayed, *Science*, 1996, **272**, 1924–1925.
93 V. Kozlovskaya, E. Kharlampieva, K. Jones, Z. Lin and V. V. Tsukruk, *Langmuir*, 2010, **26**, 7138.
94 V. V. Tsukruk and D. H. Reneker, *Polymer*, 1995, **36**, 1791–1808.
95 N. Elsner, F. Dubreuil and A. Fery, *Phys. Rev. E: Stat., Nonlinear, Soft Matter Phys.*, 2004, **69**, 031802.
96 E. Kharlampieva, D. Zimnitsky, M. Gupta, K. N. Bergman, D. L. Kaplan, R. R. Naik and V. V. Tsukruk, *Chem. Mater.*, 2009, **21**, 2696–2704.
97 E. Kharlampieva, J. M. Slocik, S. Singamaneni, N. Poulsen, N. Kroeger, R. R. Naik and V. V. Tsukruk, *Adv. Funct. Mater.*, 2009, **19**, 2303–2311.
98 V. Izumrudov, E. Kharlampieva and S. A. Sukhishvili, *Biomacromolecules*, 2005, **6**, 1782–1788.

